Turkish Journal of Electrical Engineering & Computer Sciences

http://journals.tubitak.gov.tr/elektrik/

Research Article

Turk J Elec Eng & Comp Sci
(2016) 24: 2498 – 2512

doi:10.3906/elk-1404-218

Content-based texture image retrieval by histogram of curvelets

Erkan USLU*, **Songül ALBAYRAK**,
Department of Computer Engineering, Faculty of Electrical-Electronics Engineering, Yıldız Technical University, Esenler, İstanbul, Turkey

Received: 12.04.2014 • **Accepted/Published Online:** 20.08.2014 • **Final Version:** 15.04.2016

Abstract: Curvelet decomposition is a multiscale analysis method defined for 2D and 3D signals that can represent curve-like features with great sparsity. A genuine method based on histograms of curvelets is proposed for content-based texture image retrieval. The accuracy of the method is analyzed for rotation invariance, curvelet scale-orientation size, and bin size. The results are given with precision-recall graphs. Experimental results on the Brodatz database show promising results for the proposed method compared to curvelet subband statistical features.

Key words: Histogram of curvelets, content-based image retrieval, Brodatz textures, Jeffrey divergence, precision recall

1. Introduction

Content-based image retrieval, a technique that uses visual contents to search images from large-scale image databases according to users' interests, has been an active and fast-advancing research area since the 1990s. During the past decade, remarkable progress has been made in both theoretical research and system development. However, there remain many challenging research problems that continue to attract researchers from multiple disciplines. This study mainly focuses on curvelet-based feature extraction and content-based texture retrieval. A genuine method called histograms of curvelets is proposed for this purpose.

The paper is organized as defining the used methods and materials in Section 2, defining the proposed method in Section 3, giving experimental results in Section 4, and providing the conclusion in Section 5. In Section 2, first the definitions of continuous curvelet transform and discrete curvelet transform are given, and then the distance and performance measures are defined. Finally in Section 2, the main texture databases used are introduced. In Section 3 the proposed method is defined and the implementations on deterministic signals and rotated texture datasets are given. In Section 4 the accuracy of the proposed method is analyzed according to the number of curvelet scales and orientations and bin size compared to statistical curvelet feature-based retrieval methods. Lastly, the optimum scale-orientation and bin sizes are investigated in Section 4 according to the accuracy of the classification.

1.1. Motivation

Curvelet decomposition can represent curve-like features with great sparsity. Reconstructions by small percentages of the curvelet coefficients result in by far greater signal-to-noise ratios compared to various other transforms with the same coefficient percentages [1]. With these properties curvelet-based feature extraction is gaining importance. Curvelet-based features are used in the field of content-based image retrieval by means of

*Correspondence: euslu@yildiz.edu.tr

subband parameter estimation of the probability distribution that the coefficients may be drawn from. Instead of estimating probability distribution parameters, utilization of histograms of curvelet subbands is proposed as a genuine method.

1.2. Related work

Textures are repeating primary patterns. Texture analysis is the measure of variations in images based on smoothness, coarseness, and regularity [2]. Texture features defined and used in the literature can be listed as cooccurrence matrices [3], run-length statistics [4], spectral measures such as Fourier transform [5] and discrete cosine transform [6], fractal dimensions [7], statistical moments [8], wavelets [9], Gabor filters [10], ridgelets [2], and curvelets [11].

Curvelet transform was first introduced by Candes and Dohono in 2000 [12]. In the literature content-based texture image retrieval based on curvelet features is gaining importance. In particular, the subband mean and variance values' cascaded feature vector is widely used as a benchmark classification result. In [13] for each subband generalized Gaussian distribution parameter estimation was carried out and cascaded distribution parameters were used as a feature vector.

1.3. Main contributions

A genuine method, namely histogram of curvelets (HoC), that utilizes histograms of absolute maximum normalized curvelet coefficients is proposed with this study in content-based texture image retrieval. The effect of coefficient normalization both spatially and in the curvelet domain is investigated on retrieval accuracy. The effects of bin size and curvelet scale-orientation sizes are also given with precision-recall graphs to define the optimum parameter values. The experimental results show that the proposed method gives promising performance compared to widely used curvelet statistical features.

In our previous work the proposed HoC method was used for synthetic aperture radar (SAR) image land-use classification [14]. That previous work concluded that the use of HoC results in better classification accuracies compared to other standard benchmark feature extraction methods used for SAR classification, as HoC utilizes spatial locality.

2. Methods and materials

In this section continuous and discrete curvelet transforms are defined, distance and performance measures for content-based image retrieval are given, and the dataset used is explained.

2.1. Curvelet transform

Multiscale directional transforms are closely related to the human visual system as the visual cortex handles images with spatial locality, orientations, and scales. Such resemblance shows the necessity of multiscale directional transforms in computer vision for interpreting images as we do. The curvelet transform is a multiscale directional transform that allows an almost optimal nonadaptive sparse representation of objects with edges [15]. The curvelet transform is used in image/video processing, seismic exploration, fluid mechanics, simulation of partial differential equations, and compressed sensing.

Curvelet transform is closely related to wedge filters, short-time Fourier transform (STFT), wavelet transform, Gabor wavelet transform, ridgelet transform, contourlet transform, and other directional wavelet transforms. In STFT the signal is decomposed into fixed-size rectangular regions in the frequency domain;

likewise, in wavelet transform, the signal is decomposed into fixed-area variable-size rectangular regions in the frequency domain. Contrary to the two previous transforms, curvelet transform enables directional decomposition by means of wedge-like tiling in the frequency domain. Gabor wavelet transform is the decomposition of the signal into elliptical directional tilings. The curvelet transform is derived from ridgelet transform and differs in being locally applied ridgelets. The ancestor ridgelet transform can optimally represent straight line-like features, whereas curvelet transform can represent curve-like features with great sparsity. Although contourlet transform can be calculated faster than curvelet transform, contourlets are in the form of discrete filter banks with directional but rectangular grids and result in more artifacts than curvelet transform [16].

Two generations of curvelet transform are defined in the literature, of which the second generation's approach enabled the use and understanding of curvelets easier. Second-generation curvelet transform is defined in two forms, which are based on unequally spaced fast Fourier transforms and wrapping of specially selected Fourier samples. Compared to first-generation curvelet transform, the second generation is faster and has complexity of $O(n^2 \log n)$ for an $n \times n$ image matrix [17].

2.1.1. Continuous curvelet transform

Continuous curvelet transform is defined in R^2 with spatial variable $\mathbf{x}$, frequency domain variable ω, frequency domain polar coordinate variables r and θ, radial window function W, and 2π periodic angular window function V. Given that W is supported for domain $(1/2, 2)$ and V is supported for domain $[-1, 1]$ and both are Meyer-like windows, it is showed that both W and V satisfy the admissibility conditions [17]. Combining W and V one gets U, which is a frequency domain polar wedge filter window function. Generalizing U for any scale 2^{-j} and any rotations θ_l the wedge filter family is obtained as given in Eq. (1). Here the parameters are taken as $r \geq 0$, $\theta \in [0, 2\pi)$, $\theta_l = 2\pi 2^{-\lfloor j/2 \rfloor} l$, and $j, l \in N_0$. It should also be noted that the rotation difference between wedge filters is achieved by the translation of V.

$$U_{j,l}(r, \theta) = 2^{-\frac{3j}{4}} W\left(2^{-j} r\right) V\left(\frac{2^{\lfloor j/2 \rfloor}(\theta - \theta_l)}{2\pi}\right) \tag{1}$$

Scale variable j is taken as greater than or equal to an arbitrary j_0 value, which is related to the coarse scale curvelet. Nondirectional coarse scale curvelet $U_{j_0}(\omega)$ can be given with the low-pass filter window W_0 in Eq. (2).

$$U_{j_0}(\omega) = 2^{-j_0} W_0\left(2^{-j_0} |\omega|\right) \tag{2}$$

The continuous curvelet transform of a signal is defined as the inverse Fourier transform of the product of the each element of the curvelet filter family (wedge filters) with the Fourier pair of the signal.

Spatially continuous curvelet transform can be given with a waveform $\varphi(\mathbf{x})$, oscillatory in one direction and low-pass in the other variable direction. Choosing as the Fourier pairs $U_{j_0}(\omega) \xrightarrow{\mathrm{F}^{-1}} \varphi(\mathbf{x})$, parabolically rescaled with D_j (Eq. (3)), rotated with R_{θ_l} (Eq. (4)), and translated with $\mathbf{k} = (k_1, k_2) \in Z^2$ (Eq. (5)), one can construct curvelets spatially. The coarse scale curvelet spatially is also given as in Eq. (6).

$$\varphi_j(\mathbf{x}) = |D_j| \varphi(D_j \mathbf{x}), D_j = \begin{pmatrix} 2^j & 0 \\ 0 & 2^{j/2} \end{pmatrix} \tag{3}$$

$$\varphi_{j,l}(\mathbf{x}) = |D_j| \varphi(D_j R_{\theta_l} \mathbf{x}), R_{\theta_l} = \begin{pmatrix} cos\theta_l & sin\theta_l \\ -sin\theta_l & cos\theta_l \end{pmatrix} \tag{4}$$

$$\varphi_{j,l,\mathbf{k}}(\mathbf{x}) = |D_j|\,\varphi\left(D_j R_{\theta_l}(\mathbf{x}-\mathbf{k})\right) \tag{5}$$

$$\varphi_{j_0,\mathbf{k}}(\mathbf{x}) = \varphi_{j_0}\left(\mathbf{x} - 2^{-j_0}\mathbf{k}\right) \tag{6}$$

Curvelet coefficients can be calculated then with the inner product of the function $f \in R^2$ and the curvelets given in Eq. (7).

$$c(j,l,\mathbf{k}) = \langle f, \varphi_{j,l,\mathbf{k}} \rangle = \int_R^{2(\mathbf{x})} \varphi_{j,l,k}^{-}(\mathbf{x})\mathbf{dx} \tag{7}$$

To obtain real-valued curvelets, wedges that are symmetric to the origin are taken into account as $U_{j,l}(r,\theta) + U_{j,l}(r,\theta+\pi)$. Combining all, the frequency domain tiling of curvelet coefficients is given in Figure 1a.

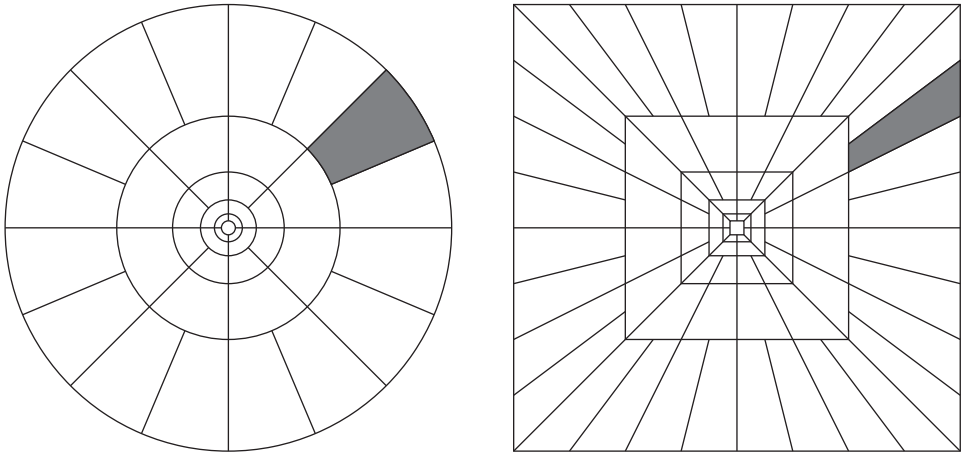

Figure 1. a) Continuous and b) discrete curvelet tilings in the frequency domain.

2.1.2. Discrete curvelet transform

Discrete curvelet transform is defined for Cartesian form functions in a similar way as in Eq. (7) and is given by Eq. (8). For the discrete curvelet transform instead of polar wedge windows shear windows are constructed from concentric squares for calculation convenience.

$$c^D(j,l,\mathbf{k}) = \sum\nolimits_{0\le t_1,t_2\le n} f[t_1,t_2]\,\varphi_{j,l,k}^{D}\bar{[}t_1,t_2] \tag{8}$$

For a function ϕ that is supported for $[-2,2]$ and ranges between $[0,1]$, a low-pass profile 2D window Φ can be constructed in the frequency domain given in Eq. (9).

$$\Phi_j(\omega_1,\omega_2) = \phi\left(2^{-j}\omega_1\right)\phi\left(2^{-j}\omega_2\right) \tag{9}$$

The Cartesian analogy of the circular window then can be given as in Eq. (10) for values of $j \ge 0$.

$$W_j(\omega) = \sqrt{\left(\Phi_{j+1}^2(\omega) - \Phi_j^2(\omega)\right)} \tag{10}$$

The angular window with all possible rotations is defined in Eq. (11).

$$V_{j,l}(\omega) = V\left(2^{\lfloor j/2 \rfloor}\omega_1/\omega_2 - l\right) \tag{11}$$

Combining W and V, one gets U, which is a frequency domain shear filter window function. Generalizing U for any scale 2^{-j} and any rotations l the shear filter family is obtained. Using a similar approach to continuous curvelets, with approximations on the shear windows, periodic wrapping, and choosing the Fourier pair as $U_{j_0}(\omega) \xrightarrow{\mathrm{F}^{-1}} \varphi^D(\mathbf{t})$, discrete curvelets can be obtained spatially. Frequency domain tiling of discrete curvelet transform is given in Figure 1b. The discrete curvelets in the spatial domain is illustrated in Figure 2 with different scale and orientation values.

The coarse curvelet coefficients are given both spatially (Figure 3a) and in the frequency domain (Figure 3b), which can be approached as a low-pass filter.

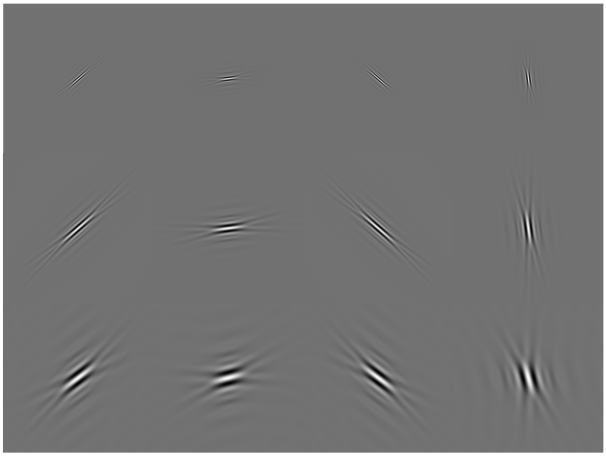

Figure 2. Curvelets spatially via warping. Left to right orientations approximately at $\mathbf{3\pi/4}$, $\mathbf{\pi/2}$, $\mathbf{\pi/4}$, 0. Top to bottom scales 4, 3, 2.

Figure 3. a) Coarse curvelet spatially. b) Coarse curvelet in the frequency domain.

2.2. Distance and performance measures

The Jeffrey divergence as a distance measure for image retrieval is defined and the overall performance measure precision-recall values are explained in subsections.

2.2.1. Jeffrey divergence

In [18], RGB (red, green, blue) histograms, RGB moments, HSV (hue, saturation, value) values, and Gabor, Tamura, and convolution-based features were tested on Corel collection with 14 different measures, given in three main categories of geometric, information theoretical, and statistical, and it was concluded that the Canberra metric, squared chord, Jeffrey divergence, and χ^2 distances were the best-performing measures. As the proposed method in this study is based on histograms and Jeffrey divergence is suitable for histogram distance, Jeffrey divergence is selected as the measure to be used based on the results in [18].

Jeffrey divergence (d_{jd}) of $A = (a_1, a_2, \cdots, a_n)$ and $B = (b_1, b_2, \cdots, b_n)$ that are the query instance and test object instance respectively can be given in Eq. (12), where $m_i = (a_i + b_i)/2$.

$$d_{jd}(A, B) = \sum_{i=1}^{n} \left(a_i \log \frac{a_i}{m_i} + b_i \log \frac{b_i}{m_i} \right) \tag{12}$$

Contrary to the widely used Kullback–Leibler divergence, Jeffrey divergence is numerically stable and symmetric [18].

2.2.2. Precision Recall

The performance of the retrieval system is measured using the standard procedure in terms of precision and recall values. Precision is the fraction of retrieved instances that are relevant, while recall is the fraction of relevant instances that are retrieved [19]. They are defined by Eqs. (13) and (14).

$$\text{Precision } (P) = \frac{\#\text{ of Relevant Retrieved}}{\#\text{ of Total Retrieved}} \tag{13}$$

$$\text{Recall } (P) = \frac{\#\text{ of Relevant Retrieved}}{\#\text{ of Total Relevant}} \tag{14}$$

The precision values for corresponding recall values for each query image are averaged over all images and the resulting precision-recall pairs are plotted as a graph with precision on the vertical axis and recall on the horizontal axis. Higher precision values for the same recall values represent better performance.

2.3. Brodatz texture images

The Brodatz database is a widely used benchmark texture dataset for content-based image retrieval [20]. The images used for the purpose of content-based texture image retrieval are taken from a web source (http://www.ux.uis.no/˜tranden/ brodatz.html). Although the dataset has 111 texture images, some are given with negative light conditions and some are similar to each other; for instance, the 'wood' main title contains tree bark, tree stump, and grain texture images and the total number of texture classes is lower than the number of images. Using the relevance between the textures from the labeling information given in [20], 60 different texture classes can be named. In this manner each image can belong to several texture classes. Given the

relevance setup mentioned it can be said that for an image there are different numbers of relevant images in the dataset.

The images are given with negative intensity mapping so images are used as intensities subtracted from 255. All of the 111 texture images are 640 × 640 pixel size except one that is 643 × 643 pixels. Images are given in 8-bit gray levels and 94 of the images' intensity values range between 0 and 255. For the rest of the images intensity values range from 10 to 230.

For the purpose of content-based texture retrieval each texture image is divided into a total of 25 nonoverlapping subimages of 128 × 128 pixels in order to increase the number of samples, so a total of 2775 texture images are obtained (Dataset I). Samples for the constructed dataset are given in Figure 4.

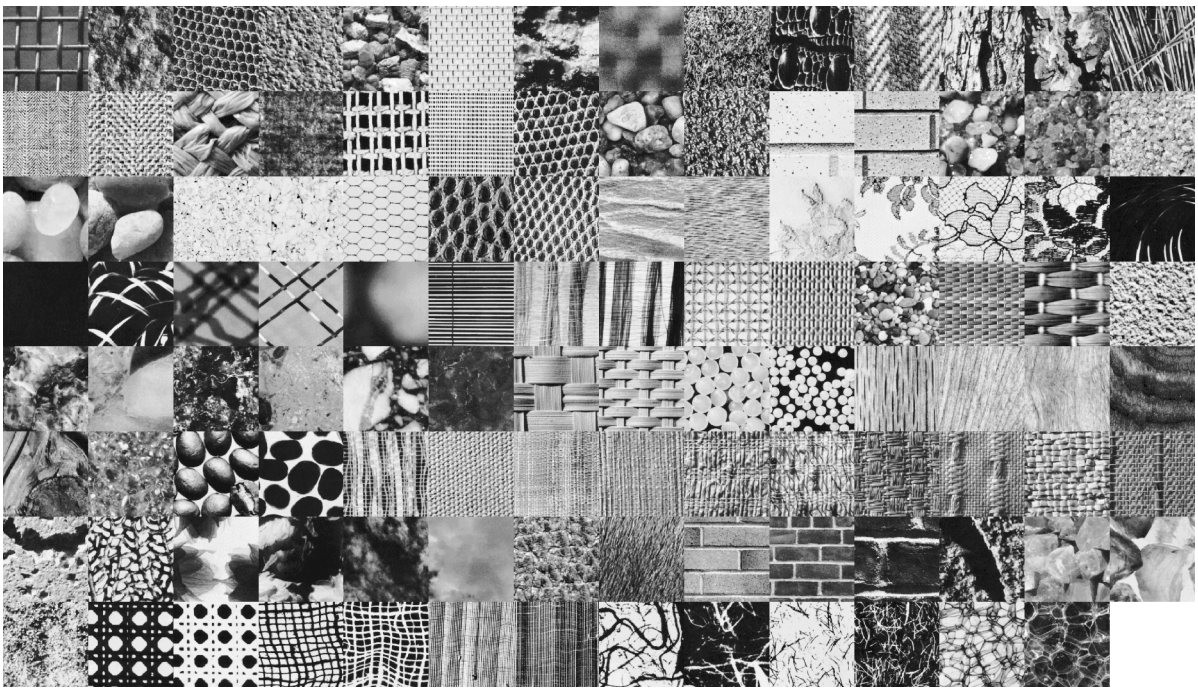

Figure 4. Brodatz samples (Dataset I).

Evaluation of rotation invariance of the proposed method is tested on a smaller dataset extracted from Brodatz given at the web source (http://sipi.usc.edu/database/database.php?volume=rotate). This dataset includes 13 textures, each of 512 × 512 pixels, and has seven different rotations of the original textures at angles of 0, 30, 60, 90, 120, 150, and 200 degrees (Dataset II). A sample from Dataset II with all rotation combinations is given in Figure 5.

Figure 5. Rotated textures Brodatz dataset sample (from Dataset II).

3. Histogram of curvelets (HoC)

Histograms are probability distributions of data for evenly or unevenly distributed intervals that give more accurate information about the dispersion of the data than mean, median, mode, standard deviation, skewness,

kurtosis, and other single-value data representations. From the point of view of probability distribution, for any random variable of a certain probability distribution, histogram calculation may give redundant data, whereas estimation of distribution variables may suffice for the parameterization. However, in practice, a physical variable cannot be fully explained even by a mixture of certain probability distributions.

Curvelet decomposition of a 2D signal is the inner product of the signal with the curvelets produced from a mother curvelet with different orientations at different scales and translations. That results in several decomposition level images, each representing curves from the original image with different sizes and orientations. Curvelet-based feature extraction then turns out to be representing curvelet decomposition images with discriminative characteristics. In this study, curvelet decomposition images are represented with cascaded subband histograms, and the distance for the feature vectors are measured by Jeffrey divergence measure.

Steps of HoC feature extraction are given in Figure 6. The first step is the curvelet transform of the input image, which is parameterized by the number of scales and number of orientations. The number of orientations determines the angle step between two consequent curvelets. As the number of scales increases, the minimum length of the curve-like feature that can be extracted decreases, resulting in better expression of the image. The AbsMax normalization step is to scale the curvelet coefficients to fit in the $[-1, 1]$ range without losing global intensity differences. This is achieved by scaling all the curvelet coefficients with the maximum absolute value of the coefficients. The histogram construction step is basically equidistant binning of the curvelet subbands. The binning step is parameterized by the number of the bins. At last the subband histograms are cascaded to form the feature vector.

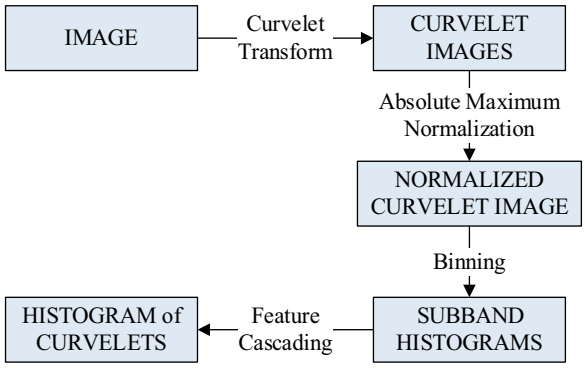

Figure 6. HoC steps.

HoC steps are carried out on two sample texture images (Figures 7a and 7b), which results in the given curvelet images (Figures 7c and 7d) and histograms (Figures 7e and 7f) illustrated in Figure 7.

3.1. HoC of deterministic signals

HoC features are extracted for predefined deterministic 2D signals in order to describe the potential and the systematic of the proposed method. Used deterministic signals are given in Figure 8, which are a sinusoid that propagates at $\hat{i}$ direction, sinusoid that propagates at $\hat{i}+\hat{j}$ direction, sinusoid that propagates at $2\hat{i}+\hat{j}$ direction, chirp at $\hat{i}$ sinusoid at $\hat{j}$, chirp that propagates at $\hat{i}+\hat{j}$ direction, chirp that propagates at $\hat{i}$ direction, sinusoid that propagates at $\hat{i}-\hat{j}$ direction, sinusoidal that propagates at $2\hat{i}-\hat{j}$ direction, chirp at $\hat{i}$ sinusoid at $-\hat{j}$, and chirp that propagates at $\hat{i}-\hat{j}$ direction (Dataset III (Figures 8a–8j).

HoC features for Dataset III are extracted with 2, 3, and 4 number of scales; 8 and 16 number of orientations; and 8, 16, 32, and 64 bin sizes. According to Jeffrey divergence the distances between deterministic

signals are calculated. The distances are arranged in order to emphasize the nearest sample to any given one by means of nearest neighbor (1NN) classification. Table 1 gives distances to each sample for 2 scales, 16 orientations, and for 8 bins.

According to Table 1, the horizontal sinusoid (Figure 8a) and horizontal chirp (Figure 8f) are closest to each other. Figures 8b and 8g, Figures 8c and 8h, and Figures 8d and 8i also show pairs that are closest to each other, which can be taken as a hint for the rotation invariance of the proposed HoC method. At any scale with fixed number of orientations considering the same signals with different elongations the curvelets also differ by the elongation, yet the histograms calculated from the curvelet coefficients are almost identical. This reasoning

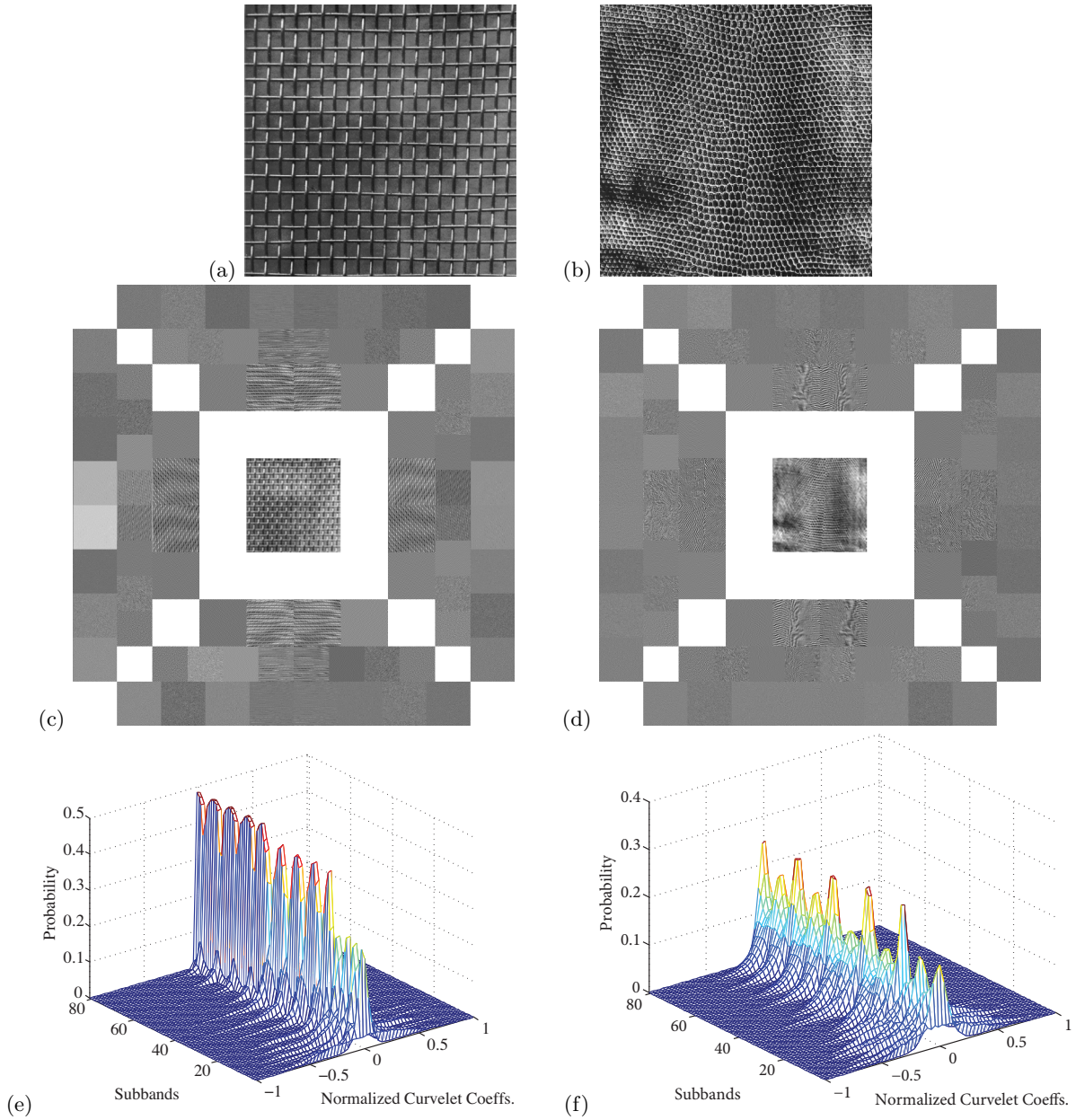

Figure 7. a, b) Texture images; c, d) absolute maximum normalized curvelet coefficients; e, f) subband histograms of curvelets.

is valid to some extent as the numbers of orientations allow similar histogram calculations. For instance Figure 8e is closest to Figure 8d and Figure 8j is closest to Figure 8i, which shows that the number of orientations overrides the rotation invariance. For 2 scales, 8 orientations, and 8 bins, the pair of Figures 8e and 8j pair is the closest to each other. Distances calculated at 2 scales, 16 orientations, and 8 bins are mostly similar to other parameter values.

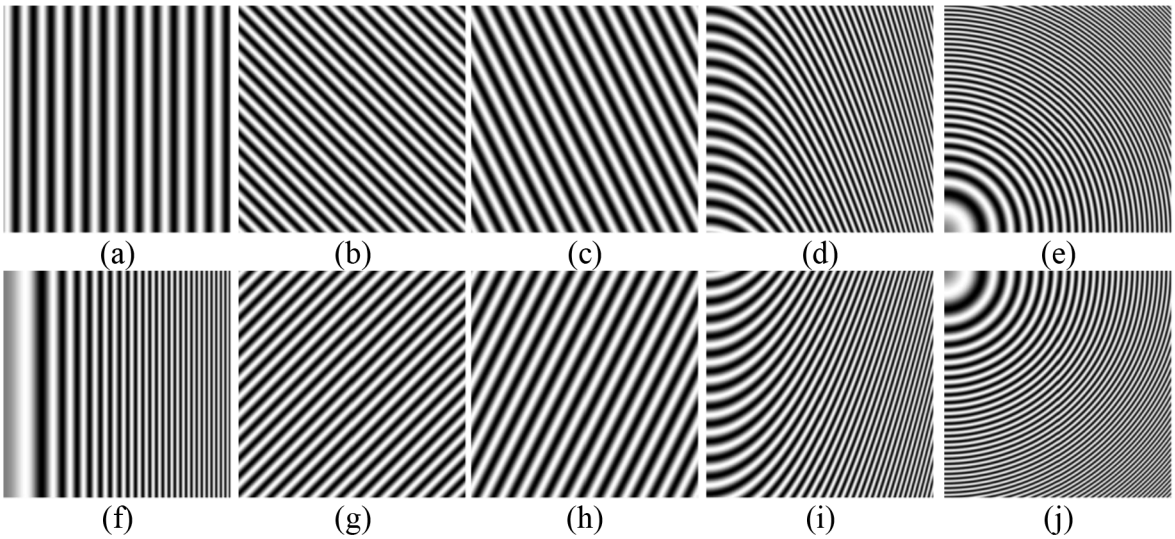

Figure 8. Deterministic 2D signals: a) sinusoid propagates at $\hat{i}$ direction, b) sinusoid propagates at $\hat{i}+\hat{j}$ direction, c) sinusoid propagates at $2\hat{i}+\hat{j}$ direction, d) chirp at $\hat{i}$ sinusoid at $\hat{j}$, e) chirp propagates at $\hat{i}+\hat{j}$ direction, f) chirp propagates at $\hat{i}$ direction, g) sinusoid propagates at $\hat{i}-\hat{j}$ direction, h) sinusoidal propagates at $2\hat{i}-\hat{j}$ direction, i) chirp at $\hat{i}$ sinusoid at $-\hat{j}$, j) chirp propagates at $\hat{i}-\hat{j}$ direction (Dataset III).

Table 1. Jeffrey distances for HoC of the deterministic signals.

	(a)	(b)	(c)	(d)	(e)	(f)	(g)	(h)	(i)	(j)
(a)	-	9.21	9.38	9.84	10.13	2.13	9.22	9.37	9.83	10.05
(b)	9.21	-	0.92	1.15	2.14	9.51	0.21	1.13	1.12	1.98
(c)	9.38	0.92	-	1.17	1.71	9.87	0.98	0.45	1.27	2.07
(d)	9.84	1.15	1.17	-	1.16	9.29	1.32	1.18	0.36	1.71
(e)	10.13	2.14	1.71	1.16	-	10.38	2.14	1.9	1.26	2.35
(f)	2.13	9.51	9.87	9.29	10.38	-	9.52	9.88	9.29	10.27
(g)	9.22	0.21	0.98	1.32	2.14	9.52	-	1.25	1.25	2.09
(h)	9.37	1.13	0.45	1.18	1.90	9.88	1.25	-	1.23	2.19
(i)	9.83	1.12	1.27	0.36	1.26	9.29	1.25	1.23	-	1.53
(j)	10.05	1.98	2.07	1.71	2.35	10.27	2.09	2.19	1.53	-

Apart from the nearest samples for each deterministic signal, the second nearest samples for Figures 8a–8j can be listed as Figure 8b, Figure 8c, Figure 8b, Figure 8b, Figure 8i, Figure 8d, Figure 8c, Figure 8b, Figure 8b, and Figure 8d, respectively.

3.2. Rotation Invariance of HoC

Dataset II is used to evaluate the rotation invariance of the proposed method with 2, 3, and 4 as number of scales; 8 and 16 as number of orientations; and 8, 16, 32, and 64 as bin sizes with Jeffrey divergence metric. For

the 91 instances (7 rotations of the original for each of the 13 textures), nearest neighbor (1NN) classification results are obtained in leave-one-out manner. The results can be read as the proposed method preserving texture features and even introducing various angle rotations to the original image. Figure 9 gives the accuracies for different scale and bin sizes. Table 2 gives an example classification result for 2 scales, 8 orientations, and 8 bins. The results also show that increase in the number of bins increases the accuracy, whereas increase in the number of scales decreases the accuracy for Dataset II.

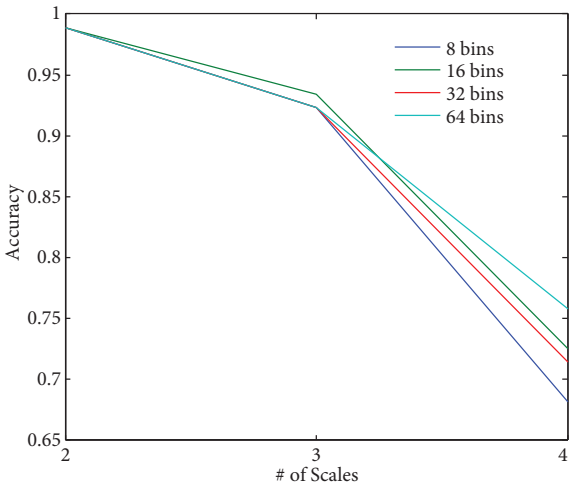

Figure 9. Dataset II accuracies for various bin and scale sizes.

Table 2. The 1NN results for HoC with different numbers of scales and orientations at 16 bins (in %).

	bark	brick	bubbles	grass	leather	pigskin	raffia	sand	straw	water	weave	wood	wool
bark	7	-	-	-	-	-	-	-	-	-	-	-	-
brick	-	7	-	-	-	-	-	-	-	-	-	-	-
bubbles	-	-	7	-	-	-	-	-	-	-	-	-	-
grass	-	-	-	7	-	-	-	-	-	-	-	-	-
leather	-	-	-	-	7	-	-	-	-	-	-	-	-
pigskin	-	-	-	-	-	6	-	-	-	-	-	-	1
raffia	-	-	-	-	-	-	7	-	-	-	-	-	-
sand	-	-	-	-	-	-	-	7	-	-	-	-	-
straw	-	-	-	-	-	-	-	-	7	-	-	-	-
water	-	-	-	-	-	-	-	-	-	7	-	-	-
weave	-	-	-	-	-	-	-	-	-	-	7	-	-
wood	-	-	-	-	-	-	-	-	-	-	-	7	-
wool	-	-	-	-	-	-	-	-	-	-	-	-	7

4. Experiments and results

The experiments are conducted on Dataset I to reveal the precision-recall accuracy of the proposed method compared with widely used statistical curvelet features. Effects of the various parameters of the proposed method, such as number of scales and orientations of the curvelet transform and the number of bins for histogram evaluation, are also analyzed comparatively. Dataset I is decomposed and labeled as it is mentioned in Section 2.3. Analysis of spatial and curvelet domain coefficient normalization is also carried out and it is concluded that the best performance is given by no normalization in the spatial domain but absolute maximum normalization

in the curvelet domain. Other tested normalization alternatives were z-normalization, absolute maximum normalization, linear normalization for the spatial domain, and subband linear normalization, z-normalization, and subband absolute maximum normalization for the curvelet domain. HoC features are calculated for 2, 3, and 4 number of scales; 8, 16, and 32 number of orientations; and 16, 32, 64, and 128 number of bins. The precision-recall graphs are calculated for the retrieval of all relevant images for any given reference image.

4.1. Effect of number of scales and orientations on HoC

Effect of number of scales and orientations for curvelet transform on HoC is analyzed for a fixed number of bins in Figure 10. Graphs are constructed for the x-axis showing different scale and orientation combinations (from right to left, 2 scales and 8 orientations, 2s 16o, 2s 32o, 3s 8o, 3s 16o, 3s 32o, 4s 8o, 4s 16o, 4s 32o); the y-axis is for recall values and the z-axis is for precision values. The results show that 3 scales and 16 orientations give the best performance for any given bin size.

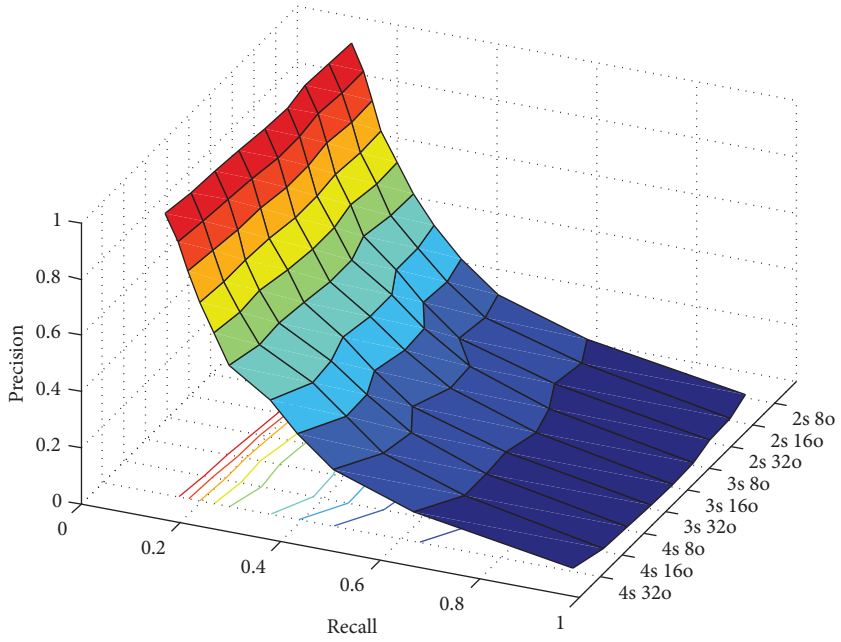

Figure 10. Effect of number of scales and orientations for various bin sizes on HoC-based retrieval.

The 1NN classification results are also supplied as a measure for effect of number of scales and orientations for HoC-based retrieval in Table 3 with a fixed number of 16 bins. These results correspond to precision values for the smallest possible recall values. The best result is obtained for 3 scales and 16 orientations.

Table 3. Confusion matrix for Dataset II with 2 scales, 8 orientations, and 8 bins, classified by 1NN.

	# of scales and orientations								
1NN HoC results	2s 8o	2s 16o	2s 32o	3s 8o	3s 16o	3s 32o	4s 8o	4s 16o	4s 32o
	91.82	94.31	94.59	95.64	95.68	95.32	93.69	93.12	91.06

4.2. Effect of bin size on HoC

Effect of bin size on HoC-based retrieval is analyzed for a fixed number of scales and orientations. For each combination of number of scales and orientations, such as 2 scales and 8 orientations, 2s 16o, 2s 32o, 3s 8o, 3s

16o, 3s 32o, 4s 8o, 4s 16o, and 4s 32o, the precision-recall graph is constructed separately with 16, 32, 64, and 128 bins. It can be seen from the results that as the number of bins increases the precision-recall graph is lifted upwards, but the positive marginal accuracy decreases. This situation is given in Figure 11 for 2 scales and 16 orientations.

4.3. Comparison of HoC with curvelet subband $\mu\sigma$ features

The best recall-precision graph for HoC is obtained for 3 scales, 16 orientations, and 16 bins as given in Figure 12 together with curvelet subband $\mu\sigma$ features for Dataset I. The benchmark $\mu\sigma$ features were described in [13] and [21] as applying curvelet transform with 4 scales and 16 orientations to the subtextures and cascading $\mu\sigma$ values for only second and third scale curvelet subbands to construct the feature vector.

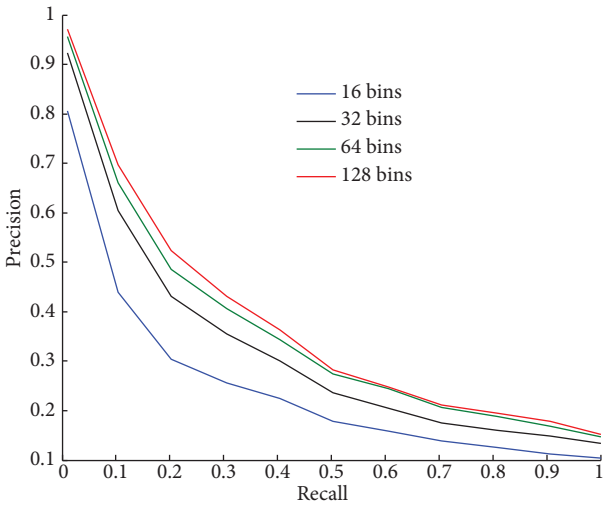

Figure 11. Effect of number of bins on HoC-based retrieval.

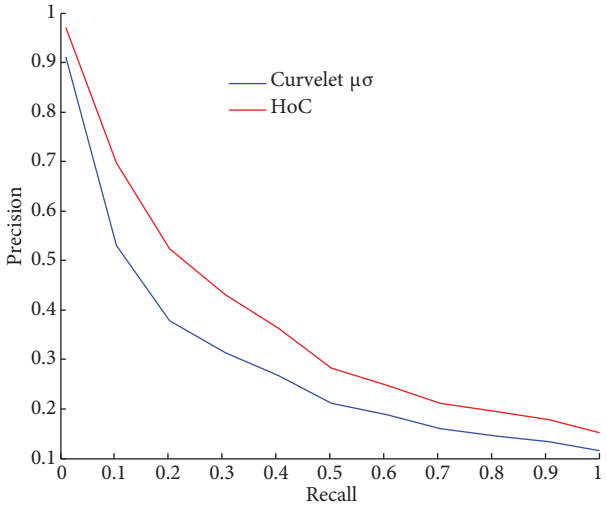

Figure 12. Comparison of HoC and μ, σ statistical curvelet features' precision-recall graphs.

As precision-recall graphs give overall performance for retrieval of all relevant images, nearest neighborhood classification results are also given by Table 3. For the proposed HoC method the 1NN classification results are given for different scale and orientation combinations for 16 histogram bins. The 1NN classification result for curvelet $\mu\sigma$ features is obtained as 86.31%.

According to Table 3, 1NN classification results for the proposed method are higher than the $\mu\sigma$ features. The best 1NN result for HoC is obtained as 95.68% for 3 scales and 16 orientations.

4.4. Retrieval results

Two of the retrieval results are given in Figure 13. The results are for the first 15 retrieved images for the given query image that is located at the top left. Retrieved images are given by texture numbers and 5 $\times$ 5 subimage locations. Figure 13a can be considered as a good retrieval result whereas retrievals in Figure 13b are from different textures other than the query images' texture.

5. Conclusion

Curvelet transform is a popular multiresolution method with great sparsity for curve-like features. In content-based texture retrieval curvelet transform was used in two different ways, such as subband μ, σ values and several

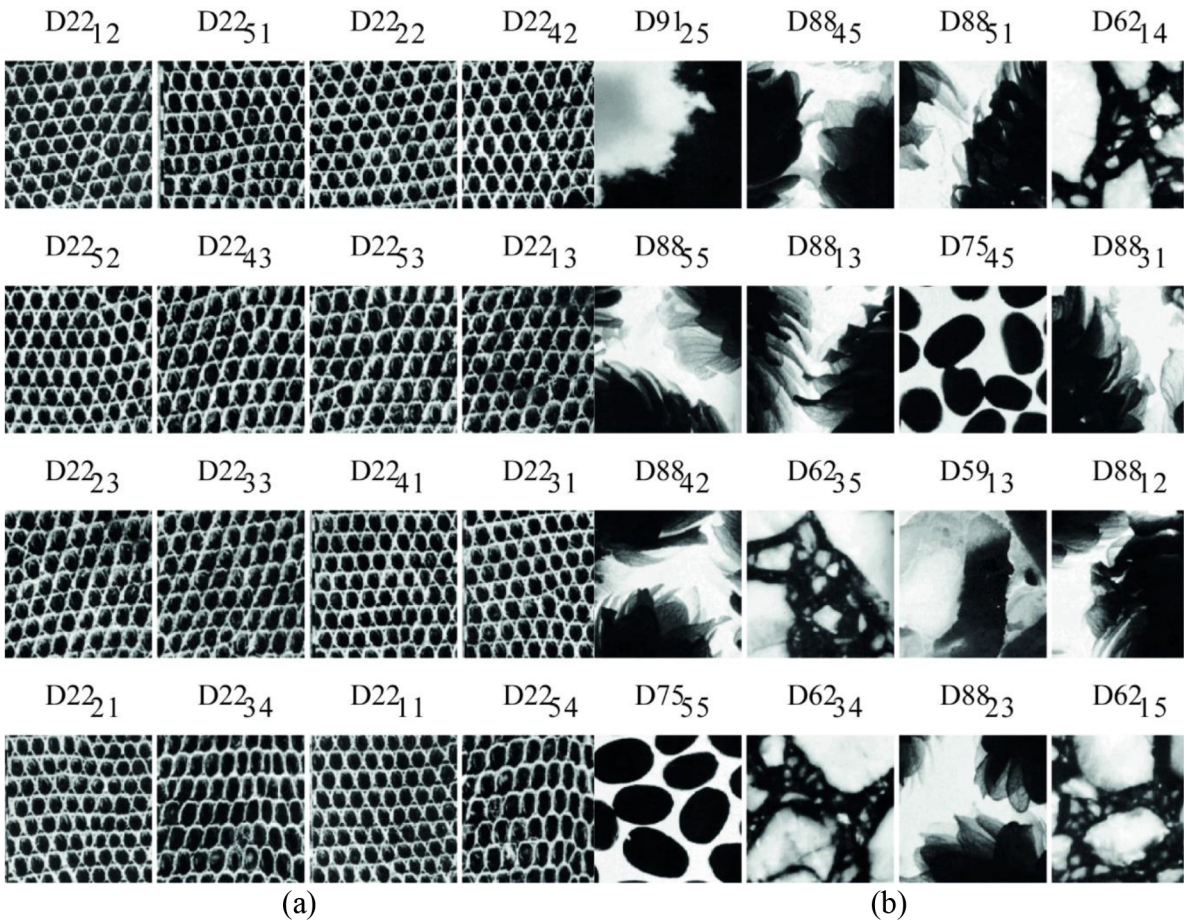

Figure 13. Retrieval results for two texture subimages (query images are located at top left): a) example of a good retrieval result, b) example of a poor retrieval result.

subband probability distribution fittings. In this work the use of absolute maximum normalized subband curvelet histograms is proposed for texture retrieval. The effects of the number of scales, number of orientations, number of bin sizes, and domain-wise normalizations are investigated on the datasets. The proposed HoC method is analyzed on the deterministic signals, rotation texture dataset, and benchmark texture dataset. Experimental results show that the proposed texture retrieval method provides rotation invariant classification to some extent and performs better than curvelet subband μ, σ features.

As a next step, the authors would like to extend the use of the proposed HoC method to other application areas such as image and hyperspectral remote sensing feature extraction. Since HoC would enable the utilization of the spatial locality, it is expected to perform better in the noisy nature of remote sensing data.

References

[1] Do MN, Vetterli M. The contourlet transform: an efficient directional multiresolution image representation. IEEE T Image Process 2005; 14: 2091-2106.

[2] Dettori L, Semler L. A comparison of wavelet, ridgelet, and curvelet-based texture classification algorithms in computed tomography. Comput Biol Med 2007; 37: 486-498.

[3] Howarth P, Rüger S. Evaluation of texture features for content-based image retrieval. Lect Notes Comput Sc 2004; 3115: 326-334.

[4] Xu DH, Kurani AS, Furst JD, Raicu DS. Run-length encoding for volumetric texture. In: The 4th IASTED International Conference on Visualization, Imaging, and Image Processing; 2004.

[5] Hervé N, Boujemaa N. Image annotation: which approach for realistic databases? In: Proceedings of the 6th ACM International Conference on Image and Video Retrieval; 2007; Amsterdam, the Netherlands. pp. 170-177.

[6] Ngo CW, Pong TC, Chin RT. Exploiting image indexing techniques in DCT domain. Pattern Recogn 2001; 34: 1841-1851.

[7] Mishra AK, Raghav S. Local fractal dimension based ECG arrhythmia classification. Biomed Signal Proces 2010; 5: 114-123.

[8] Aptoula E. Comparative study of moment based parameterization for morphological texture description. J Vis Commun Image R 2012; 23: 1213-1224.

[9] Datta R, Joshi D, Li J, Wang JZ. Image retrieval: ideas, influences, and trends of the new age. ACM Comput Surv 2008; 40: 5:1-5:60.

[10] Liu Y, Zhang D, Lu G, Ma WY. A survey of content-based image retrieval with high-level semantics. Pattern Recogn 2007; 40: 262-282.

[11] Islam MM, Zhang D, Lu G. Region based color image retrieval using curvelet transform. Lect Notes Comput Sc 2010; 5995: 448-457.

[12] Candès EJ, Donoho DL. Curvelets, multiresolution representation, and scaling laws. Proc SPIE 2000; 4119: 1-12.

[13] Gómez F, Romero E. Rotation invariant texture characterization using a curvelet based descriptor. Pattern Recogn Lett 2011; 32: 2178-2186.

[14] Uslu E, Albayrak S. Curvelet-based synthetic aperture radar image classification. IEEE Geosci Remote S 2014; 11: 1071-1075.

[15] Ma J, Plonka G. The curvelet transform. IEEE Signal Proc Mag 2010; 27: 118-133.

[16] Do MN. Contourlets and sparse image expansions. Proc SPIE 2013; 5207: 560-570.

[17] Candès E, Demanet L, Donoho D, Ying L. Fast Discrete Curvelet Transforms. 2005. Available online at http://www.curvelet.org/papers/FDCT.pdf.

[18] Liu H, Song D, Rüger S, Hu R, Uren V. Comparing dissimilarity measures for content-based image retrieval. In: Proceedings of the 4th Asia Information Retrieval Conference on Information retrieval Technology; 2008; Harbin, China. pp. 44-50.

[19] Singha M, Hemachandran K, Paul A. Content-based image retrieval using the combination of the fast wavelet transformation and the colour histogram. IET Image Process 2012; 6: 1221-1226.

[20] Brodatz P. Textures: A Photographic Album for Artists and Designers. New York, NY, USA: Dover Publications, 1966.

[21] Sumana IJ, Islam MM, Zhang D, Lu G. Content based image retrieval using curvelet transform. In: 10th IEEE Workshop on Multimedia Signal Processing; 2008. pp. 11-16.